B-Cell Depletion Attenuates White and Gray Matter Pathology in Marmoset Experimental Autoimmune Encephalomyelitis

Kap, Yolanda S.; Bauer, Jan; van Driel, Nikki; Bleeker, Wim K.; Parren, Paul W. H. I.; Kooi, Evert-Jan; Geurts, Jeroen J. G.; Laman, Jon D.; Craigen, Jenny L.; Blezer, Erwin

Published in:
Journal of neuropathology and experimental neurology

DOI:
10.1097/NEN.0b013e318234d421

Publication date:
2011

J Neuropathol Exp Neurol
Vol. 70, No. 11
November 2011
pp. 992–1005

ORIGINAL ARTICLE

B-Cell Depletion Attenuates White and Gray Matter Pathology in Marmoset Experimental Autoimmune Encephalomyelitis

Yolanda S. Kap, PhD, Jan Bauer, PhD, Nikki van Driel, BSc, Wim K. Bleeker, MD, PhD, Paul W.H.I. Parren, PhD, Evert-Jan Kooi, MSc, Jeroen J.G. Geurts, PhD, Jon D. Laman, PhD, Jenny L. Craigen, PhD, Erwin Blezer, PhD, and Bert A. 't Hart, PhD

Abstract

This study investigated the effect of CD20-positive B-cell depletion on central nervous system (CNS) white and gray matter pathology in experimental autoimmune encephalomyelitis in common marmosets, a relevant preclinical model of multiple sclerosis. Experimental autoimmune encephalomyelitis was induced in 14 marmosets by immunization with recombinant human myelin oligodendrocyte glycoprotein in complete Freund adjuvant. At 21 days after immunization, B-cell depletion was achieved by weekly intravenous injections of HuMab 7D8, a human–anti-human CD20 antibody that cross-reacts with marmoset CD20. In vivo magnetic resonance imaging showed widespread brain white matter demyelination in control marmosets that was absent in CD20 antibody–treated marmosets. High-contrast postmortem magnetic resonance imaging showed white matter lesions in 4 of the 7 antibody-treated marmosets, but these were significantly smaller than those in controls. The same technique revealed gray matter lesions in 5 control marmosets, but none in antibody-treated marmosets. Histologic analysis confirmed that inflammation, demyelination, and axonal damage were substantially reduced in brain, spinal cord, and optic nerves of CD20 antibody–treated marmosets. In conclusion, CD20-postive B-cell depletion by HuMab 7D8 profoundly reduced the development of both white and gray matter lesions in the marmoset CNS. These data underline the central role of B cells in CNS inflammatory-demyelinating disease.

Key Words: B cell, *Callithrix jacchus*, Demyelination, Experimental autoimmune encephalomyelitis, Multiple sclerosis, Ofatumumab, Rituximab.

INTRODUCTION

Multiple sclerosis (MS) is a long-term neurologic disease characterized by inflammation and demyelination in central nervous system (CNS) white matter (WM) and gray matter (GM) (1, 2). It is generally believed that CNS pathology involves an (auto)immune attack mediated by CD4-positive and CD8-positive T cells, macrophages, and autoantibodies (3). Recent studies have highlighted a prominent pathogenic role for B cells in MS that could not be explained by removal of the source of autoantibody production, suggesting other pathogenic mechanisms mediated by B cells (4–6). Depletion of B cells with the chimeric anti–CD20 antibody rituximab has reduced the relapse rate in patients with relapsing-remitting MS (RRMS) (4, 5, 7). The remarkable clinical effect of B-cell depletion in RRMS was supported by the demonstration using magnetic resonance imaging (MRI) that the total number and volume of T2 lesions and the number of new gadolinium-enhancing brain WM lesions were significantly reduced (4, 5).

This study was undertaken to obtain proof-of-principle that B cells are a valid target for antibody-mediated therapy, aiming at the prevention of injury to CNS WM and GM. We investigated this in a valid preclinical MS model, experimental autoimmune encephalomyelitis (EAE) in common marmosets (8, 9). This model is characterized by widespread demyelination of both WM and GM that mimics the pathologic findings in MS patients (10, 11). The experiment was performed with 2 groups of marmosets in which EAE was induced by a single immunization with recombinant human myelin oligodendrocyte glycoprotein (rhMOG) in complete Freund adjuvant. In 1 group, depletion of CD20-positive B cells was induced at 21 days after immunization using a human–anti-human CD20 antibody (HuMab 7D8) (12, 13). This antibody induces profound and long-lasting depletion of CD20-positive B cells from the circulation and lymphoid organs of marmosets (14). The second group received placebo

From the Department of Immunobiology (YSK, NvD, BAtH), Biomedical Primate Research Centre, Rijswijk; MS Centre ErasMS (YSK, JDL, BAtH), Rotterdam, the Netherlands; Center for Brain Research (JB), University of Vienna, Austria; Genmab (WKB, PWHIP), Utrecht; Departments of Pathology (EJK, JJGG) and Anatomy and Neurosciences (EJK, JJGG), VU University Medical Center, Amsterdam; Department of Immunology (YSK, JDL), Erasmus MC, University Medical Center, Rotterdam, the Netherlands; GSK Discovery (JLC), BioPharm R&D, Stevenage, United Kingdom; Image Sciences Institute (EB), University Medical Center Utrecht, Utrecht; and Department of Medical Physiology (BAtH), University Medical Center Groningen, the Netherlands.

Send correspondence and reprint requests to: Yolanda S. Kap, PhD, Department of Immunobiology, Biomedical Primate Research Centre, PO Box 3306, 2280 GH Rijswijk, the Netherlands; E-mail: kap@bprc.nl

Drs Blezer and 't Hart contributed equally to this work.

The authors report the following financial interests: at the time the study was executed, Drs Parren and Bleeker were employed by Genmab BV, Utrecht, the Netherlands; and Dr Craigen is an employee of GlaxoSmithKline, Stevenage, UK. The study was financed via an unbiased grant from GlaxoSmithKline and by funding from the Netherlands Organization for Scientific Research.

Supplemental digital content is available for this article. Direct URL citations appear in the printed text and are provided in the HTML and PDF versions of this article on the journal's Web site (www.jneuropath.com).

treatment with an equivalent volume of phosphate-buffered saline (PBS). Treatment was started late after priming to model intervention in an ongoing immunopathogenic process, while achieving complete B-cell depletion before disease onset in early EAE responders (15).

The immunologic changes caused by CD20-positive B-cell depletion in marmoset EAE, that is, marked changes in autoantibody levels as well as T-cell activation and cytokine profiles, have been reported (14). Here, we report the dramatic effects on the CNS pathology.

MATERIALS AND METHODS

Animals

Healthy adult common marmoset monkeys used in this study (n = 14) were randomly selected from the outbred colony at the Biomedical Primate Research Centre (Rijswijk, the Netherlands) (Table 1). Included animals had been determined to be healthy by routine physical, hematologic, and biochemical examinations by a veterinarian. The mean body weights of the marmosets in the control and treatment groups were 321 ± 30 and 342 ± 49 g, respectively. The marmosets were pair-housed under conventional conditions in spacious cages and were under intensive veterinary observation throughout the study. The daily diet consisted of commercial food pellets for New World monkeys (Special Diet Services, Witham, Essex, UK), supplemented with raisins, marshmallows, biscuits, and fresh fruit. Drinking water was provided ad libitum. All study protocols and experimental procedures were reviewed and approved by the institute's ethics committee before the start of the study according to the Dutch law on animal experimentation. All animal studies were carried out in accordance with EU directive 86/609/EEC and GSK Policy on the Care, Welfare, and Treatment of Laboratory Animals.

Experimental Autoimmune Encephalomyelitis Induction

Experimental autoimmune encephalomyelitis was induced with a recombinant protein encompassing the extracellular domain of human MOG produced in *Escherichia coli* (residues 1–125; rhMOG) and purified as previously described (16). The inoculum contained 100 μg of rhMOG in 300 μl of PBS emulsified with 300 μl of complete Freund adjuvant (containing *Mycobacterium butyricum*; Difco Laboratories, Detroit, MI). The 600-μl emulsion was injected at 4 locations into the dorsal skin under alfaxalone anesthesia (10 mg/kg; alfaxan; Vetoquinol, Den Bosch, the Netherlands).

Clinical signs were scored daily by 2 independent observers using a previously described semiquantitative scale (17). Briefly, 0 = no clinical signs; 0.5 = apathy, altered walking pattern without ataxia; 1 = lethargy, tail paralysis, tremor; 2 = ataxia, optic disease; 2.25 = monoparesis; 2.5 = paraparesis, sensory loss; 3 = paraplegia or hemiplegia; 4 = quadriplegia; and 5 = death due to EAE. For ethical reasons, marmosets were killed once complete paralysis of hind limbs (EAE score 3.0) was observed, or at the predetermined end point of the study, which was arbitrarily set at 15 weeks.

Marmosets selected for necropsy were first deeply sedated by intramuscular injection of alfaxalone (10 mg/kg) followed by infusion of pentobarbital sodium (Euthesate; Apharmo, Duiven, the Netherlands).

TABLE 1. Animals and Clinical Scores

					Postsensitization Day‡		
Monkey	**Pair**	**Sex**	**Age, mo***	**Body Weight, g†**	**Score 2**	**Score 3**	**End**
Control							
M02052	1	M	84	307	46	—	59
M06061	2	M	31	306	41	54	55
M06081§		M	28	283	—	—	33
M07021	3	M	24	339	66	83	83
M07029	4	M	24	377	78	91	91
M07048	5	M	21	316	71‖, 84‖, 88‖	—	105
M07080	6	M	20	322	66	73	73
CD20 antibody treatment							
M04096	1	M	56	308	41‖, 43‖	—	104
M05073	2	M	43	430	—	—	106
M06055§	2	M	31	333	—	—	106
M07012	3	M	26	330	—	—	105
M07075	4	M	21	374	103‖	—	106
M07085	5	M	20	273	—	—	104
M07095	6	M	19	347	46‖	—	105

*Age in months at the start of the experiment.
†Body weight (g) at the start of the experiment.
‡Survival time to score 2: p = 0.0291; survival time to death (with clinical signs ≥2): p = 0.0021.
§M06081 died on postsensitization day 33 without EAE by cardiac arrest and was excluded from further analysis. M06055 was added to pair 2 for magnetic resonance imaging.
‖Score 2 for 1 day.
M, male.

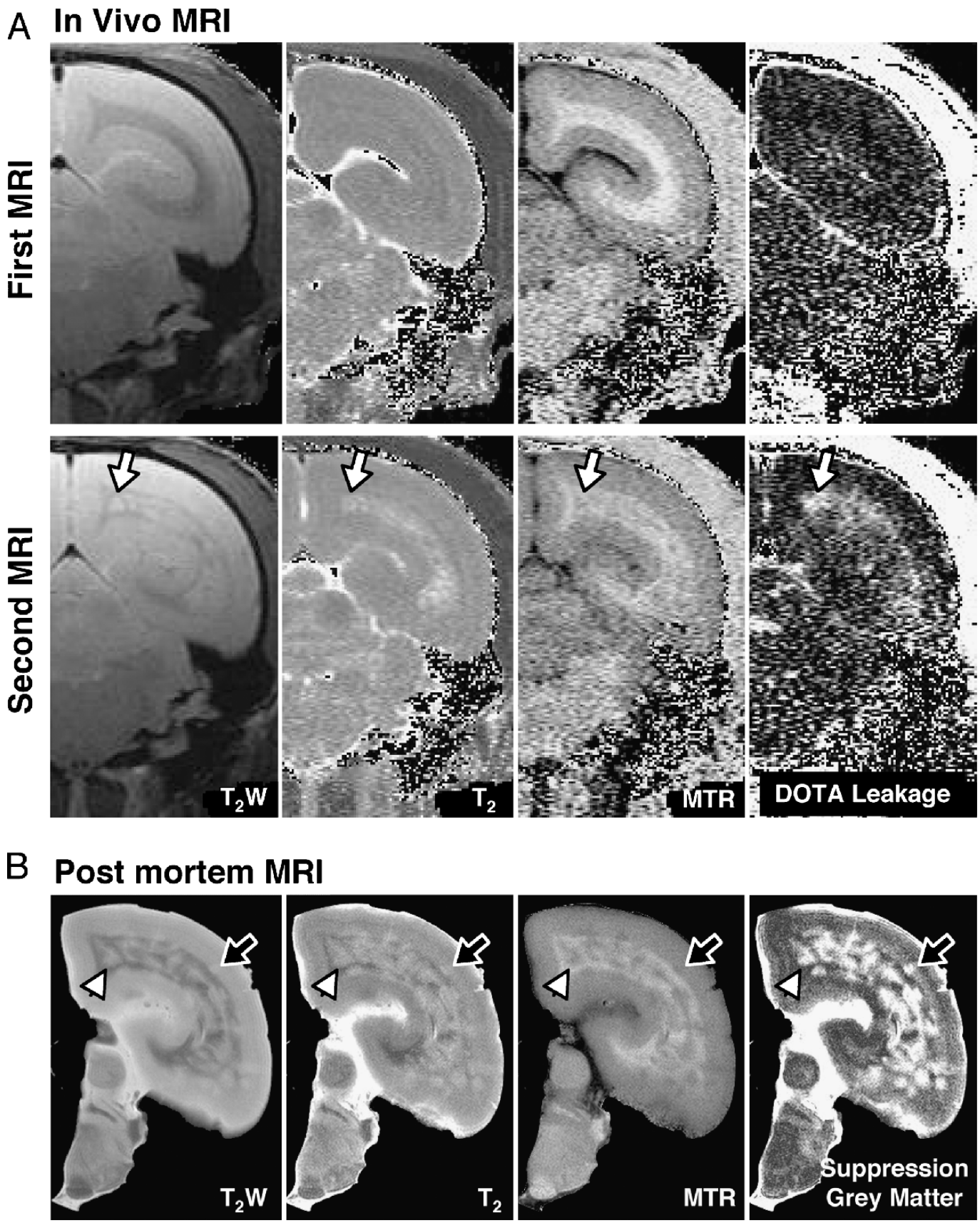

CD20 Antibody Treatment

HuMab 7D8 is a human IgG1κ monoclonal antibody directed against human CD20 (12, 13) that cross-reacts with marmoset CD20 (data not shown). Seven marmosets received a single intravenous dose of 20 mg/kg HuMab 7D8 at postsensitization day (PSD) 21 to induce robust B-cell depletion from blood and lymph nodes. To maintain plasma trough levels of HuMab 7D8 greater than 5 to 10 μg/ml (18), 5 mg/kg was administered intravenous every week. The 7 control animals received a weekly intravenous injection with 1 mL/kg sterile PBS (Table 1).

Magnetic Resonance Imaging

In vivo experiments were performed using a 4.7-T horizontal bore nuclear magnetic resonance spectrometer (Varian, Palo Alto, CA) after sedation of the animal with alfaxalone (10 mg/kg). Imaging sequences included quantitative T_2 relaxation time (T_2), magnetization transfer ratio (MTR), and Gadovist leakage imaging. White matter lesions, WM, normal-appearing WM (NAWM), and GM areas were defined for calculation of MR characteristics. White matter was measured as total WM in the first caudal to rostral slice that showed the complete corpus callosum. Normal-appearing WM was defined in this slice as the WM minus the WM lesions present in this slice. The WM parameter represents total WM and, therefore, includes NAWM as well as WM lesions. In animals in which WM lesions were absent, no NAWM was calculated because this is the same as WM. See also supplemental methods for a detailed description (Appendix, Supplemental Digital Content 1, http://links.lww.com/NEN/A275).

For postmortem imaging, 1 cerebral hemisphere collected at necropsy was fixed in 4% buffered formalin and transferred after 14-day fixation into buffered saline containing sodium azide to stabilize MR relaxation time characteristics (19). Brains were submerged in nonmagnetic oil (Fomblin; perfluorinated polyether; Solvay Solexis, Weesp, the Netherlands) to prevent unwanted susceptibility artifacts. High-contrast postmortem MR images were recorded on a 9.4-T horizontal bore nuclear magnetic resonance spectrometer (Varian) equipped with a quadrature coil (RAPID; Biomedical, Rimpar, Germany). T_2 and MTR images were collected as described in supplemental methods (Appendix, Supplemental Digital Content 1, http://links.lww.com/NEN/A275). Inversion recovery, in which the signal from the GM was suppressed, was performed to facilitate the detection of GM lesions. Image resolution was more than 10 times higher than the resolution obtained with in vivo MRI. Next to the areas described previously, GM lesions and normal-appearing GM areas were also outlined (Appendix, Supplemental Digital Content 1, http://links.lww.com/NEN/A275).

Histology and Immunohistochemistry

Frozen and fixed tissues were processed for examination with histologic and immunohistochemical techniques as previously described (20–22). Sections were stained with Luxol fast blue–periodic acid–Schiff stain and by immunohistochemistry for myelin proteolipid protein (PLP), MRP14, MHC class II, CD3, CD20, complement C9neo, IgG, and SMI-32. The CD20 antibody used to stain B cells reacts with another epitope than HuMab 7D8.

Analysis of Demyelination

Demyelination was assessed as follows: brain sections stained for PLP were photographed at 2.5× magnification; images were then imported in the Scion Image program (freeware downloaded from www.scioncorp.com), an image processing and analysis program based on NIH Image developed at the National Institutes of Health, Bethesda, MD. In density slice mode, first the total area of the section was measured. After this, total WM (approximately 40 mm^2) was measured and subtracted from the total area, resulting in the GM area (approximately 100 mm^2). Lesions in WM and GM were selected by freehand mode, and their sizes were measured. Finally, the demyelination in WM or GM was calculated as percentage of total WM or GM. For the spinal cords, 8 sections from each animal (amounting to approximately 6 cm^2 in total) were analyzed. Demyelination in optic nerve was scored as follows: + = demyelination, ± = some demyelination, − = no demyelination.

Statistics

Data are presented as mean ± SEM of 6 control and 7 treated marmosets. Statistical analysis was performed using GraphPad Prism 5.0b for Mac OS X. Survival was analyzed using log-rank test. Differences between control and treated marmosets were analyzed using the Mann-Whitney U test. Differences between WM lesions and WM or NAWM within the control group were analyzed by the paired Student t-test. $p < 0.05$ was considered significant.

RESULTS

Clinical Course and In Vivo Brain MRI Recording

One marmoset (M06081) from the control (PBS-treated) group died unexpectedly at PSD 33 from cardiac failure and was therefore excluded from further analyses. Clinical analysis of EAE development in 6 control and 7 antibody-treated monkeys showed that depletion of CD20-positive B cells significantly prevented the development of clinical signs (14)

FIGURE 1. Overview of magnetic resonance imaging (MRI) of a control marmoset (M06061) that developed severe experimental autoimmune encephalomyelitis. **(A)** No abnormalities were detected on the images during the first in vivo MRI measurement, that is, postsensitization day (PSD) 18 (upper row). The second in vivo MRI (second row; PSD 41) showed typical MRI abnormalities associated with the presence of white matter (WM) lesions, that is, increased T_2 signal intensity, decreased magnetization transfer ratio (MTR), and increased tetraazacyclododecanetetraacetic acid (DOTA) leakage values. The white arrow points to a typical WM lesion. **(B)** In the postmortem images, which are obtained with more than 10 times higher resolution, the lesion identified in **(A)** (white arrowhead) is also shown. Gray matter lesions (black arrow) are also visible on the postmortem image, particularly when the signal arising from the gray matter is suppressed. T2W = T2-weighted.

(Table 1, survival time to score 2: $p = 0.0291$; survival time to death with clinical signs: $p = 0.0021$).

Before the start of the experiment, the animals were paired based on age and body weight. Of each pair, 1 monkey received control substance and 1 monkey the therapeutic antibody (Table 1). The first MRI was planned before the start of the treatment, at PSD 18. When at least 1 monkey of a pair had experienced evident neurologic signs (clinical score ≥2), a second MRI was made of both paired monkeys to assess whether the 2 monkeys had a different brain lesion load.

At PSD 18, none of the animals showed MRI-detectable brain lesions, although the presence of small nonfocal pathologic alterations invisible with the applied MRI techniques could not formally be excluded (Fig. 1A). In 4 pairs, neurologic signs (score ≥2) were first observed in the control monkey, whereas at that time, the 4 paired HuMab 7D8–treated monkeys had no neurologic signs (pairs 2, 3, 4, and 5). The MRI of the other 2 pairs was made because the treated animal (pair 6) or both animals (pair 1) displayed clinical score 2. In 4 of the 6 control animals, WM lesions were detected at the second MRI (Table 2 and Fig. 1A). There were no detectable brain WM lesions in 2 control animals (i.e. M07021 and M07080); the latter was asymptomatic at the day the MRI was made. Brain lesions were detected with in vivo MRI in none of the HuMab 7D8-treated animals, although two animals (M04096 and M07095) had experienced a short episode of clinical score 2 (1 day) only a few days before the MRI was made (Table 2).

In Vivo MRI Analysis

Several clinically relevant MRI parameters were quantitated in WM, NAWM, GM, and WM lesion areas (Figure, Supplemental Digital Content 2, http://links.lww.com/NEN/A276). Typical MRI characteristics of WM lesions, namely, increased T_2, decreased MTR, and increased Gadovist leakage compared with WM or NAWM, were found in control animals (Table 3; Table, Supplemental Digital Content 3, http://links.lww.com/NEN/A277). In controls, the MTR was significantly lower in WM lesions than in NAWM, which is compatible with the presence of inflammation and demyelination. No WM lesions were observed in HuMab 7D8–treated animals. We compared WM of treated animals with NAWM of controls because they both reflect WM without WM lesions, but differences between NAWM of control and WM of treated animals were not statistically significant.

The increment of T1 signal intensity by intravenous Gadovist was somewhat lower in the WM of HuMab 7D8–treated animals than in WM and NAWM of control animals, suggesting that there is a higher overall increase of blood-brain barrier (BBB) permeability throughout the complete WM in the control animals. The permeability of the BBB, as indicated by albumin deposition, was observed in the brain parenchyma of both control and treated animals (data not shown). No statistically significant differences between the groups were observed for the GM with respect to volume, T_2, MTR, or Gadovist leakage (Table 3; Table, Supplemental Digital Content 3, http://links.lww.com/NEN/A277).

In conclusion, these data demonstrate that depletion of CD20-positive B cells 3 weeks after EAE induction prevented the development of detectable WM lesions in vivo.

Postmortem MRI of the Brain

To maximize the detection of EAE-associated pathology, formalin-fixed brain hemispheres were examined with high-resolution MRI at 9.4-T field strength. The voxel volume of the postmortem images was more than 10-fold higher than for the in vivo images (7.2 vs 97.6×10^{-3} mm^3), thereby facilitating the detection of small lesions. Gray matter lesions were also detectable in these images, particularly when the MR signal of GM was suppressed (Figure, Supplemental Digital Content 2, http://links.lww.com/NEN/A276).

The MR scans revealed the presence of WM lesions in all 6 control animals with the typical characteristics of significantly increased T_2 and significantly decreased MTR signals in WM lesions versus WM or NAWM (Fig. 1B and Table 4; Table, Supplemental Digital Content 4, http://links.lww.com/NEN/A278). Small WM lesions were observed in 4 of the 7 treated animals, but the average WM lesion volume of the treatment group was significantly lower than that of the control group (Table 4; Table, Supplemental Digital Content 4, http://links.lww.com/NEN/A278). Although 4 HuMab 7D8–treated animals had WM lesions, their T_2 values were significantly lower, and the MTR values were higher compared with the WM lesions in control animals. Furthermore, T_2 and MTR values of WM lesions did not significantly differ from WM or NAWM in treated animals,

TABLE 2. Brain White Matter Lesion Volume and Timing of the Second In Vivo MRI

		Control-Treated			CD20 Antibody–Treated		
Pair	PSD MRI	Animal No.	PSD Score 2	Lesion Volume, mm^3	Animal No.	PSD Score 2	Lesion Volume, mm^3
1	48	M02052	46	22	M04096	41*, 43*	0
2	48	M06061	41	591	M05073		0
					M06055		0
3	73	M07021	66	0	M07012		0
4	85	M07029	78	8	M07075	103*	0
5	85	M07048	71*, 84*, 88*	2	M07085		0
6	50	M07080	66	0	M07095	46*	0

*Score 2 for 1 day.
MRI, magnetic resonance imaging; PSD, postsensitization day.

TABLE 3. Volume, T_2, MTR, and Gadovist Leakage During the Second In Vivo Brain MRI

	Treatment	
	Control	CD20 Ab
Volume, mm^3		
WM	51.0 ± 2.8	45.7 ± 2.8
GM	96.1 ± 3.3	97.2 ± 1.4
NAWM	43.6 ± 9.4	—*
WM lesion†	104.0 ± 97.4	0.00‡
T_2 (ms)		
WM	58.04 ± 2.62	55.53 ± 0.68
GM	59.76 ± 0.63	60.86 ± 0.84
NAWM	55.47 ± 0.68	—*
WM lesion	63.95 ± 3.06	—*
MTR (% decrease signal intensity)		
WM	42.33 ± 1.15	43.81 ± 0.51
GM	32.18 ± 0.17	32.01 ± 0.41
NAWM	42.97 ± 0.77	—*
WM lesion	36.48 ± 1.04§	—*
Gadovist leakage (% increase signal intensity)		
WM	7.30 ± 1.03	6.02 ± 0.27
GM	7.98 ± 0.33	7.65 ± 0.25
NAWM	7.26 ± 1.01	—*
WM lesion	13.31 ± 2.91	—*

Shown are mean ± SE.

*Not determined because of the absence of WM lesions.

†Lesion volumes were determined in the total brain; WM, GM, and NAWM values were only determined for a single predefined slice, that is, the first caudal to rostral slice that showed the complete corpus callosum connection. Consequently, WM lesion volumes can be larger than the WM/NAWM volume.

‡, $p < 0.05$ versus the control group with the Mann-Whitney U test.

§, $p < 0.05$, paired Student t-test was used to compare MTR values of WM lesions versus NAWM of the 4 control animals with WM lesions (see also Table, Supplemental Digital Content 3, http://links.lww.com/NEN/A277).

GM, gray matter; MRI, magnetic resonance imaging; MTR, magnetization transfer ratio; NAWM, normal-appearing white matter; WM, white matter.

in contrast to control animals. These data suggest that the lesions of treated animals had less myelin damage.

Gray matter lesion formation was detected in 5 of the 6 control animals, but in none of the HuMab 7D8–treated animals (Fig. 1B and Table 4; Table, Supplemental Digital Content 4, http://links.lww.com/NEN/A278). Differences in MR characteristics between GM lesions and surrounding unaffected tissue (GM/normal-appearing GM) were much lower than the differences observed for WM lesions versus NAWM (WM/NAWM). Thus, depletion of CD20-positive B cells not only reduced the development of WM lesions but also prevented the development of GM lesions.

CNS WM Pathology

Histologic analysis revealed actively demyelinating brain lesions in all control animals, even in the animals that had only small MRI-detectable lesions on the postmortem images (M07029 and M07080). By contrast, the small WM lesions detected with high-contrast postmortem MRI in 4 HuMab 7D8–treated animals showed no histologic signs of active demyelination (Table 5; Table, Supplemental Digital Content 4, http://links.lww.com/NEN/A278). Demyelination in the spinal cord was observed in 5 of the 6 control animals but in only 2 of the 7 treated animals. The percentage demyelination was significantly smaller in treated animals. Demyelination in the optic nerve was observed in 4 of the 6 control but in none of the treated animals (Figs. 2A–F and Table 5).

Many inflammatory lesions were observed in the brains of all 6 control animals. Despite the absence of demyelination in the brain, 4 of the 7 HuMab 7D8–treated animals had some small inflammatory lesions. This explains the detection of some small lesions by high-contrast postmortem MRI in the absence of demyelination. In the spinal cord, 5 of the 6 control animals had prominent inflammation in the spinal cord. Spinal cord lesions were undetectable in the control animal that was killed without clinical signs at the end of the study (M07048). Spinal cord lesions were also absent in 4 of the 7 antibody-treated animals and were small in the other 3. The number of B and T cells was determined in spinal cord. As expected, no B cells were observed in the spinal cord of HuMab 7D8–treated animals. T cells were observed in all control animals and in 6 of the 7 HuMab 7D8–treated animals. The number of T cells in these treated animals was, in some cases, higher than in the control animals, for example, in M07085 (43.1 CD3-positive cells/mm^2), but the average number of T cells was less in HuMab 7D8–treated

TABLE 4. Postmortem MRI of 1 Brain Hemisphere

	Treatment	
	Control	CD20 Ab
Volume, mm^3		
WM	23.0 ± 1.9	18.8 ± 1.2
GM	36.4 ± 2.9	40.8 ± 1.5
NAWM	15.4 ± 2.4	17.1 ± 1.3
NAGM	35.1 ± 3.4	—*
WM lesion†	103.6 ± 56.1	0.2 ± 0.1‡
GM lesion†	9.7 ± 9.0	0.0‡
T_2 (ms)		
WM	29.56 ± 0.93	28.03 ± 0.96
GM	33.66 ± 1.11	34.81 ± 1.49
NAWM	28.45 ± 0.70	28.03 ± 0.96
NAGM	34.18 ± 1.20	—*
WM lesion	34.93 ± 0.78§	30.19 ± 0.70‡
GM lesion	35.33 ± 1.27	—*
MTR (% decrease signal intensity)		
WM	33.98 ± 1.52	36.69 ± 0.34
GM	22.46 ± 0.22	22.25 ± 0.37
NAWM	35.40 ± 0.90	36.79 ± 0.58
NAGM	22.49 ± 0.27	—*
WM lesion	28.83 ± 0.91§	32.18 ± 1.79
GM lesion	24.33 ± 0.78	—*

Shown are mean ± SEM.

Data of the individual animals are included in Table, Supplemental Digital Content 4, http://links.lww.com/NEN/A278.

*Could not be determined because of the absence of GM lesions.

†Note that lesion volumes were determined in the total brain, whereas WM, GM, and NAWM values were only determined for a single predefined slice. See also Table 3.

‡, $p < 0.05$ compared with the control group with the Mann-Whitney U test.

§, $p < 0.05$, paired Student t-test was used to compare MTR values of WM lesions versus NAWM of the 6 control animals with WM lesions.

GM, gray matter; MRI, magnetic resonance imaging; MTR, magnetization transfer ratio; NAGM, normal-appearing gray matter; NAWM, normal-appearing white matter; WM, white matter.

TABLE 5. Neuropathology of Brain, Spinal Cord, and Optic Nerve

	Brain			Spinal Cord				Optic Nerve	
		Demyelination†							
	Inflammation*	WM, %	GM, %	Inflammation*	CD3, Cells/mm^2	CD20, Cells/mm^2	Demyelination, %	Inflammation*	Demyelination†
Control									
M02052	2	27	1	1	61	6.3	13	+	+
M06061	2	42	5	3.2	31.8	15.3	36	+	+
M07021	2	2	0	2.3	36.3	16.6	44	−	±
M07029	2	3	0	1.7	27.7	8.5	64	−	−
M07048	2	9	0.5	0	1.0	0.0	0	±	±
M07080	2	5.5	0	1.3	20.8	6.7	37	−	−
Mean		14.75	1.08	1.583	29.77	8.9	32.33		
SEM		6.61	0.80	0.45	8.03	2.525	9.30		
CD20 Ab									
M04096	1	0	0	0	0	0	0	−	−
M05073	0	0	0	0	2.8	0	0	−	−
M06055	0	0	0	0	15.2	0	0	−	−
M07012	0	0	0	0	0.5	0	0	−	−
M07075	1	0	0	0.5	26.8	0	4	−	−
M07085	1	0	0	0.3	43.1	0	0	−	−
M07095	1	0	0	0.2	3.1	0	2	−	−
Mean		0‡	0	0.143‡	13.07	0‡	0.86‡		
SEM		0	0	0.08	6.23	0	0.60		

*Inflammation was visualized by staining infiltrating cells with hematoxylin and eosin, CD3, CD20, or MRP14. The inflammatory index of the spinal cord is given as the average number of inflamed blood vessels/spinal cord cross section. Inflammation in the optic nerve is assessed by staining macrophages with MRP14: + = macrophages present, ± some macrophages present, − = no macrophages. Inflammation in the brain is assessed as follows: 0 = no lesions, 1 = some small lesions, 2 = many lesions.

†Demyelination was visualized by staining myelin and myelin degradation products with Klüver Barrera or by immunohistochemistry with an antibody against myelin proteolipid protein (PLP) and assessed as described in Materials and Methods.

‡, $p < 0.05$ compared with the control group.

GM, gray matter; WM, white matter.

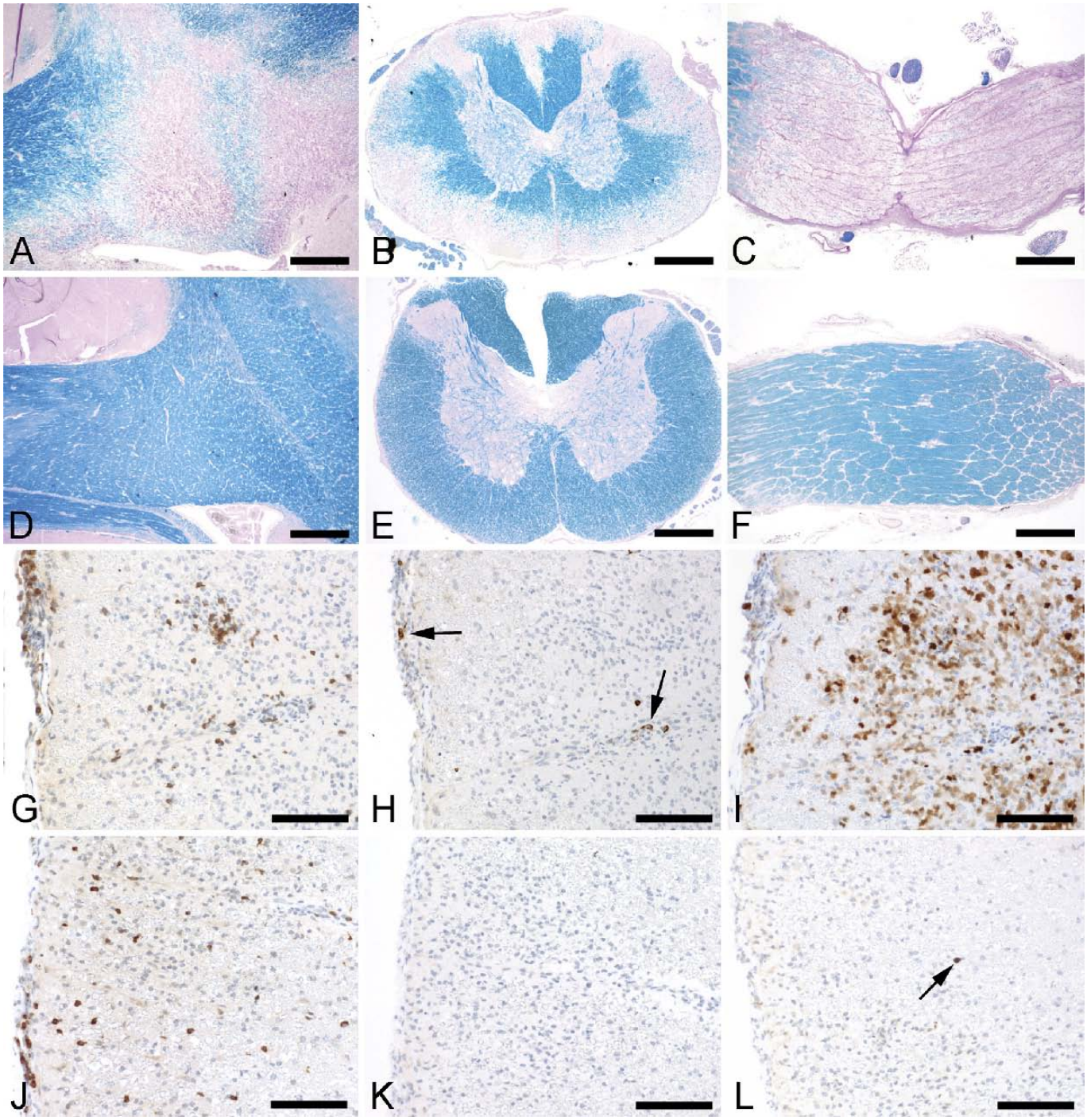

FIGURE 2. B-cell depletion reduces demyelination and inflammation in the white matter. **(A–C)** Luxol fast blue staining for myelin shows demyelination in the brain **(A)**, spinal cord **(B)**, and optic nerve **(C)** of a representative control animal. **(D–F)** There is minimal or no demyelination in the brain **(D)**, spinal cord **(E)**, and optic nerve **(F)** of a HuMab 7D8–treated animal. **(G–I)** Immunohistochemistry for CD3-positive T cells **(G)**, CD20-positive B cells **(H**, arrows indicate some cells in meninges and perivascular space**)** and MRP14-positive macrophages/microglia **(I)** in the spinal cord of an untreated animal. **(J–L)** In the spinal cord of a HuMab 7D8–treated animal CD3-positive T cells were detected **(J)**, but there are no CD20-positive B cells **(K)**. Apart from a single cell (arrow), MRP14-positive macrophages/microglia are absent in this lesion **(L)**. Bars = 500 μm **(A–F)**; 100 μm **(G–L)**.

animals than in control animals (Table 5). Macrophages were profoundly reduced in the spinal cord of HuMab 7D8–treated animals but were clearly present in control animals (Figs. 2G–L). Deposition of IgG and C9neo was observed in brain and spinal cord of control animals, but not in HuMab 7D8–treated animals (data not shown), suggesting

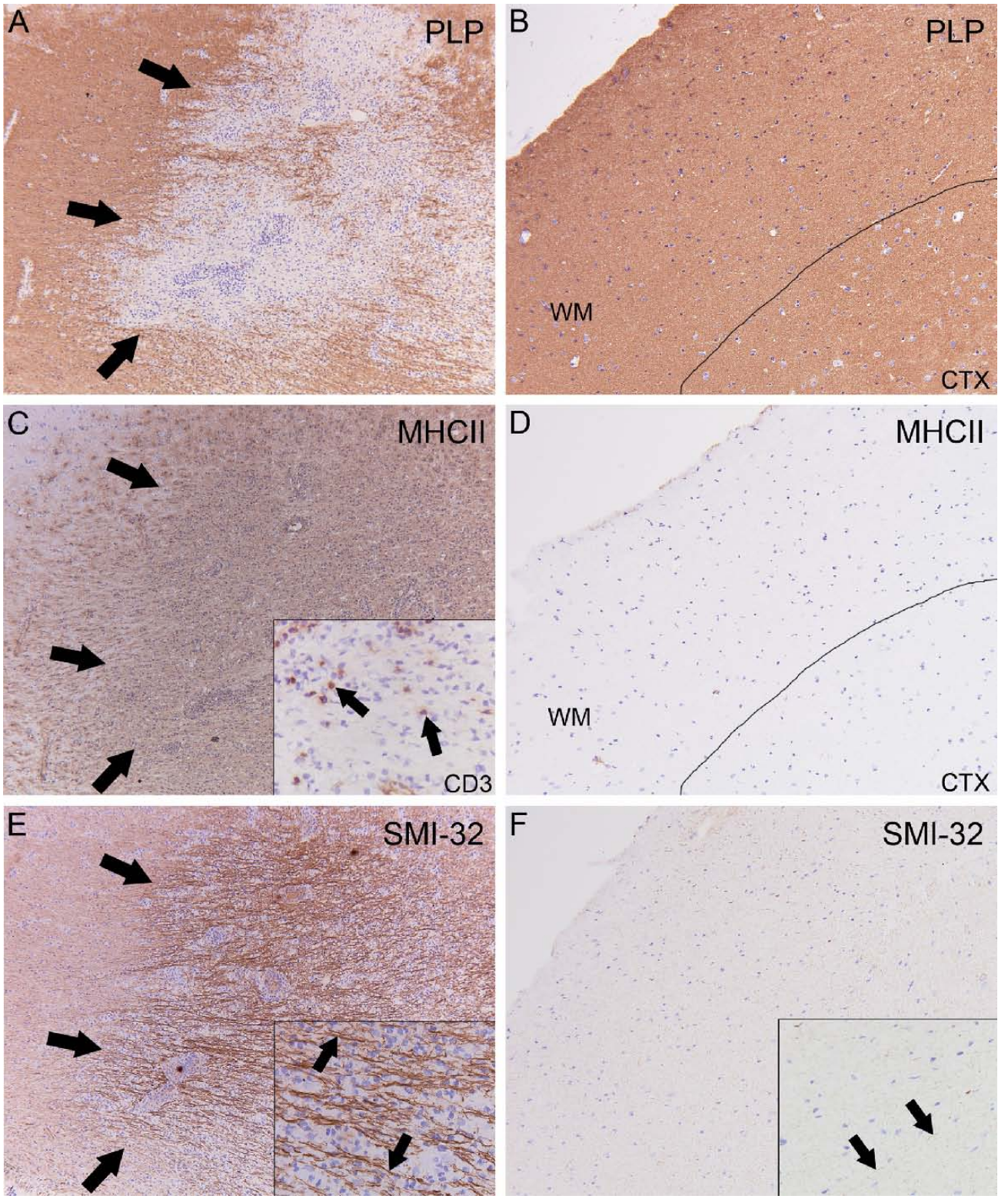

FIGURE 3. B-cell depletion prevents axon damage in the white matter (WM). **(A–F)** A representative example of a control animal **(A, C, E)** and a HuMab 7D8–treated animal **(B, D, F)**. Anti–myelin proteolipid protein (PLP) staining shows a lesion in the WM of a control marmoset **(A)**; no lesions were observed in the treated animals **(B)**. The WM lesion of the control animal contained MHC class II–positive cells **(C)** and T cells **(C**, inset**)**; no inflammatory cells were observed in treated animals **(D)**. SMI-32 positivity was observed in the lesion of the control animal **(E)**, but this was less obvious in the treated animal **(F)**. Arrows mark the border of the demyelinated lesion. Arrows in the insets of **E** and **F** indicate SMI-32–positive axons. CTX, cortex.

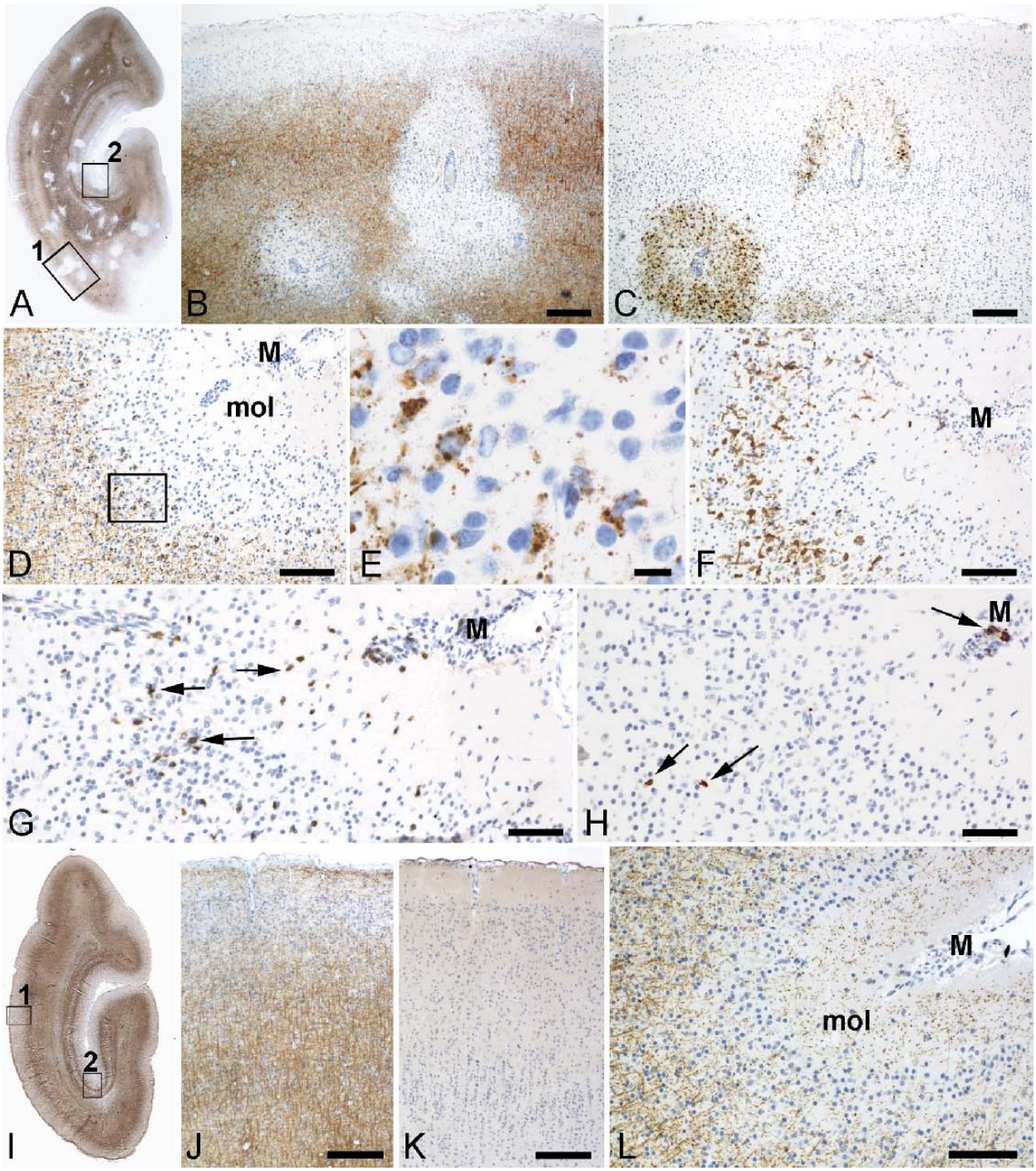

FIGURE 4. B-cell depletion prevents the development of gray matter lesions. **(A–H)** Control animal. An overview of myelin proteolipid protein (PLP) staining demonstrates multiple demyelinated areas in the cortex **(A)**. There are 2 intracortical lesions in the rectangle indicated by 1 shown at higher magnification in **(B**, bar = 200 μm**)**. The same lesions are stained for MRP14-positive macrophages/microglia in **C**. The subpial lesion indicated by rectangle 2 in **A** is shown in **D** to **F**. Note the absence of PLP-positive fibers in the molecular layer (mol) **(D)**. M = meninges. The rectangle in **D** indicates an area with active demyelination and the presence of macrophages/microglia with PLP-positive degradation products, which is enlarged in **E** (bar = 10 μm). **(F)** MRP14-positive macrophages/microglia. **(G)** CD3-positive T cells in the meninges and parenchyma (arrows). **(H)** Some CD20-positive B cells (arrows) in the same area as in **D**. Bar = 100 μm **(D**, **F–H)**. **(I–L)** B-cell depletion prevents the development of gray matter lesions in a HuMab 7D8–treated animal. Staining for PLP shows the cortex at low magnification **(I)**. The rectangles indicated by 1 and 2 show areas enlarged in **J** (area 1; bar = 200 μm) and **L** (area 2; bar = 100 μm). In both areas, PLP-positive myelin is intact. There are prominent thinly myelinated fibers in the molecular layer of **L**. M, meninges; Mol, molecular layer. **K** (bar = 200 μm) shows the absence of MRP14-positive macrophages/microglia in the same area as in **J**.

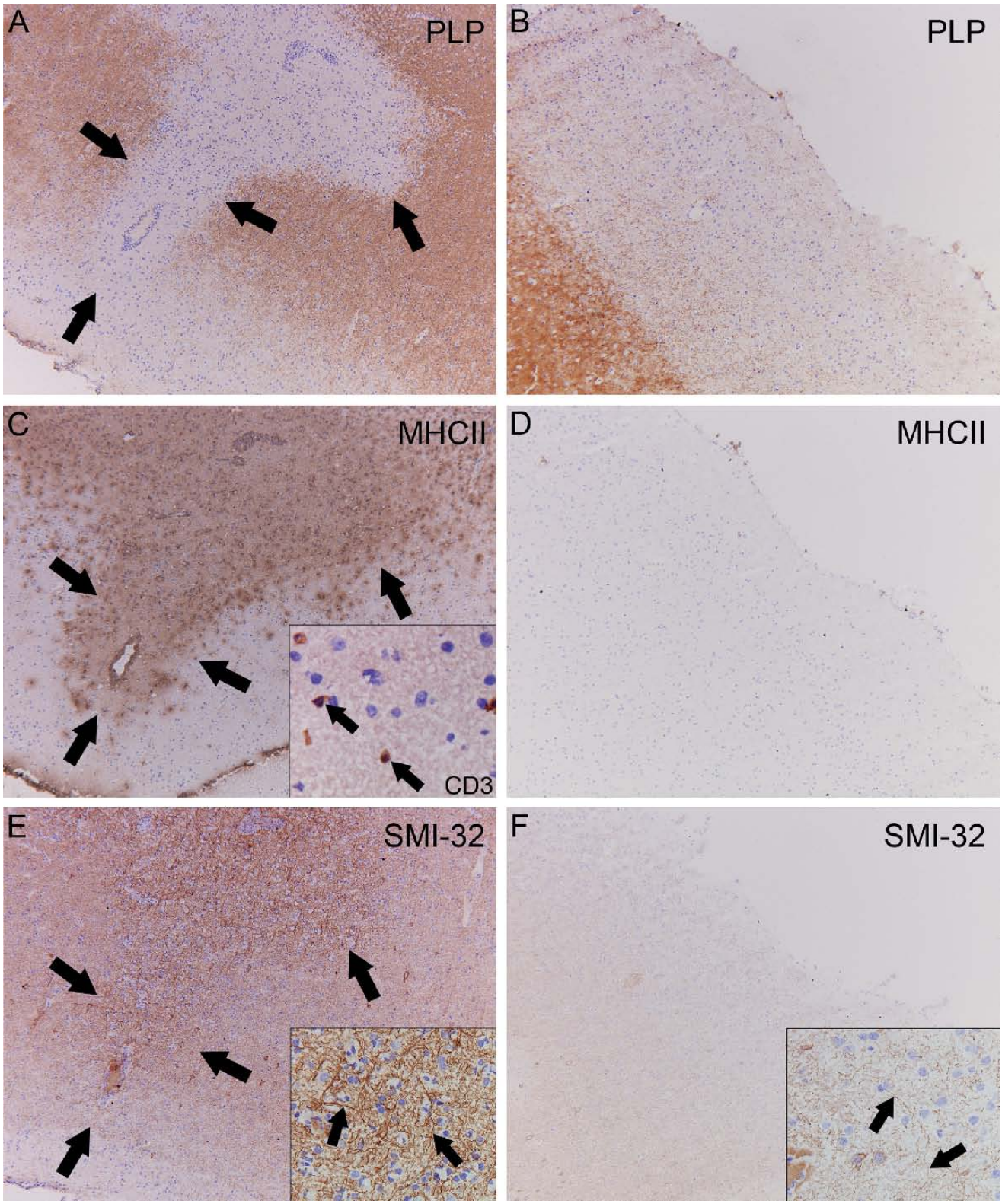

FIGURE 5. Absence of axon damage in the cerebral cortex after B-cell depletion. **(A–F)** Axonal damage in representative control **(A, C, E)** and B-cell–depleted **(B, D, F)** animals. Anti–myelin proteolipid protein (PLP) staining shows a cortical lesion in the control **(A)**, with MHC class II–positive cells **(C)**, and T cells **(C**, inset**)**. Axon damage in this lesion is shown with SMI-32 staining **(E)**. No demyelination **(B)**, inflammatory cells **(D)**, or axonal damage **(F)** was observed in B-cell–depleted animals. Arrows mark the border of the demyelinated lesion. Arrows in the insets of **E** and **F** indicate SMI-32–positive axons.

that antibody-mediated immunity is absent in HuMab 7D8–treated animals. Overall, the severity of inflammation in the spinal cord was significantly higher in control animals than in the HuMab 7D8–treated animals. Inflammation in the optic nerve was detected in 3 of the 6 controls but in none of the treated animals (Table 5).

Although it is uncertain whether axonal damage can occur in the absence of demyelination, we investigated whether axonal damage occurs in control and B-cell depleted animals. Figure 3 shows a representative example of a control and a HuMab 7D8–treated marmoset. A demyelinating WM lesion of a control marmoset is shown containing many MHC class II–positive cells and T cells. Increased immunopositivity was found for the axonal damage marker SMI-32 (23) in this lesion. Only low SMI-32 immunoreactivity was observed in the treated animals, suggesting that limited axonal damage was present. Overall, these data suggest that B-cell depletion reduces demyelination, inflammation, and axonal damage in the WM.

Gray Matter Pathology

Gray matter demyelination in the marmoset EAE model can be substantially more extensive than the usually focal demyelination in WM (Fig. 4). Note that lesions in the depicted control animal were not only observed in the cortical GM but also in the hippocampus (Figs. 4A, B). Gray matter lesions were detected in 5 control animals by MRI and in 3 of these animals, this was confirmed by histology. Histologic analysis confirmed the MRI observation that no GM lesions could be found in the HuMab 7D8–treated animals (Fig. 4 and Table 5; Table, Supplemental Digital Content 4, http://links.lww.com/NEN/A278). The cortical lesions in the control animals consist of PLP-phagocytosing macrophages/microglia, T cells, and B cells (Figs. 4C–H). In contrast, no demyelination or MRP14-positive macrophages/activated microglia were observed in the treated animals (Figs. 4I–L).

Gray matter lesions in control animals are positive for SMI-32, indicating axonal damage. Less SMI-32 positivity was observed in HuMab 7D8–treated animals (Fig. 5). Thus, depletion of CD20-positive B cells dramatically attenuated the development of MS-like pathology affecting WM and GM in all parts of the marmoset CNS.

DISCUSSION

Clinical trials in RRMS patients have shown marked clinical benefits of CD20-positive B-cell depletion by rituximab, including a reduction of relapse frequency and contrast-enhancing lesions in the cerebral WM (4, 5). As a first step toward understanding the presumed multifaceted pathogenic role of B cells in CNS-demyelinating disease, we investigated the effect of CD20-positive B-cell depletion in the rhMOG-induced EAE model in marmosets. This model is characterized by MS-like lesions developing in CNS WM and GM, which may be induced by the synergistic action of autoreactive T cells and autoantibodies (9, 10, 15, 24).

We found that the depletion of CD20-positive B cells, which was induced well after EAE induction, led to protection against clinical EAE and reduced the total volume of brain WM lesions. In addition, there was suppression of demyelination in the optic nerve and in spinal cord similar to that shown in a mouse EAE model (25). B-cell depletion not only reduces lesion volume but also changes the pathologic features of the lesions, that is, macrophages, complement, and antibodies were absent in the lesions.

The most important finding in the current study is the complete absence of demyelination and axonal damage in the GM. To our knowledge, this is the first documented evidence that GM pathology can be prevented with a CD20-positive B-cell depleting antibody. Cortical GM pathology is a relatively recently recognized aspect of the complex MS pathology that may contribute to cognitive impairment (2, 26). The pathology of GM lesions differs from WM lesions in a low number of lymphocytes, low level of complement deposition, and the absence of BBB disruption (27–29). However, there is marked activation of microglia at the borders of GM lesions (27, 30). The pathogenic processes underlying GM lesions are still unknown, but several mechanisms have been proposed (2). Gray matter lesions may start in the GM via a different pathogenic process than WM lesions or they are a consequence of damage in the WM. Although the role of B cells in GM lesion pathogenesis is unknown and their number is lower in GM lesions than in WM lesions, this study indicates that B cells are intimately engaged in the development of GM lesions. The association of meningeal B-cell follicles with severe cortical pathology in secondary progressive MS might be one explanation as to how B-cell depletion prevents GM pathology, but further research is needed (31).

The mechanisms via which B cells contribute to MS and which mechanisms are affected by B-cell depletion are not known. The most investigated role of B cells in MS is autoantibody production. According to a widely supported concept, autoimmune demyelination in MS can take place in the absence (pattern 1 lesion) or presence (pattern 2 lesion) of IgG antibody binding to myelin (32). This view is strongly supported by findings in the marmoset EAE model (15, 33–35). Although anti-CD20 treatment does not target plasma cells, anti-MOG IgG is reduced in the circulation of mice and marmosets in which B cells were depleted (14, 25, 36, 37). In addition, no IgG or C9neo deposition was observed in the CNS of HuMab 7D8–treated marmosets. This may partly explain the reduced demyelination observed, but in the rituximab trials in RRMS, significant reduction of total serum IgG levels was not found; however, the specific effect on antimyelin antibodies has not been determined (4, 5). The authors of these articles speculate that serum IgG levels were not affected by rituximab because plasma cells do not express CD20 and were therefore not depleted (38). This raises the question as to whether the clinical effect is mediated by another mechanism via which B cells can induce demyelination.

One mechanism that may be affected by B-cell depletion is the production of B-cell cytokines. It has been demonstrated that B cells in MS patients exhibit increased production of lymphotoxin and tumor necrosis factor (6, 39). As suggested by Lund and Randall (40), it may also be that B-cell depletion disrupts the feed-forward loop between B cells and T cells leading to more regulatory T cells. As a consequence repopulated B cells will also be regulatory. Indeed, several studies show that regulatory B cells can protect against EAE (25, 41).

B cells may also function as antigen presenting cells leading to T-cell activation. Reduced T-cell activity after CD20-positive B-cell depletion has been observed in various experimental systems, including naive mice, NOD mice, 2 mouse models for arthritis, and mice infected with *Listeria monocytogenes* (42, 43). We have previously reported that the expression of clinical signs of EAE is associated with the activation of a unique subset of cytotoxic IL-17A producing T cells, which mediate widespread CNS demyelination in the absence of anti-MOG antibodies (15, 35). Separately, we have reported the observation that B-cell depletion by HuMab 7D8 significantly reduced T-cell proliferation and cytokine production in spleen and lymph nodes of rhMOG-immunized marmosets (the same animals as used in the present study) (14). Importantly, the number of T cells that could be observed in the CNS of HuMab 7D8–treated animals was reduced. Similar results have been observed in mouse EAE models, namely, both T_H1 and T_H17 cell numbers were reduced in spleen and CNS (36, 37). Because demyelination in EAE-affected marmosets can occur in the absence of autoantibodies directed against rhMOG and MOG peptides, we hypothesize that the abrogation of CNS injury after B-cell depletion might be caused by the prevention of the activation of autoreactive T cells. This hypothesis is supported by our recent observation that similar results were obtained after B-cell depletion in an antibody-independent EAE model, that is, EAE in marmosets induced by MOG34-56 in IFA (15).

In conclusion, B-cell depletion effectively prevents the development of inflammation, demyelination, and axonal damage in the brain WM and GM as well as in spinal cord and optic nerve. This emphasizes that CD20-positive B cells have a central pathophysiologic role in inflammation, demyelination, and axonal damage and are an important target of therapies aiming at abrogation of lesion development in all areas of the CNS.

ACKNOWLEDGMENTS

The authors thank Fred Batenburg, Mariska van Etten, and Martine Hoffmann for their excellent biotechnical assistance and daily care of the animals; Jaco Bakker, DVM, for expert veterinary care; and Tom Haaksma and Dr Ivanela Kondova for autopsy of the animals. The authors also thank Henk van Westbroek for the artwork and Dr Ed Remarque for statistical advice.

REFERENCES

1. Compston A, Coles A. Multiple sclerosis. Lancet 2008;372:1502–17
2. Geurts JJ, Barkhof F. Grey matter pathology in multiple sclerosis. Lancet Neurol 2008;7:841–51
3. Sospedra M, Martin R. Immunology of multiple sclerosis. Annu Rev Immunol 2005;23:683–747
4. Hauser SL, Waubant E, Arnold DL, et al. B-cell depletion with rituximab in relapsing-remitting multiple sclerosis. N Engl J Med 2008;358:676–88
5. Bar-Or A, Calabresi PA, Arnold D, et al. Rituximab in relapsing-remitting multiple sclerosis: A 72-week, open-label, phase I trial. Ann Neurol 2008;63:395–400
6. Bar-Or A, Fawaz L, Fan B, et al. Abnormal B-cell cytokine responses a trigger of T-cell–mediated disease in MS? Ann Neurol 2010;67:452–61
7. Hawker K, O'Connor P, Freedman MS, et al. Rituximab in patients with primary progressive multiple sclerosis: Results of a randomized double-blind placebo-controlled multicenter trial. Ann Neurol 2009;66:460–71
8. 't Hart BA, Massacesi L. Clinical, pathological, and immunologic aspects of the multiple sclerosis model in common marmosets (*Callithrix jacchus*). J Neuropathol Exp Neurol 2009;68:341–55
9. Kap YS, Laman JD, 't Hart BA. Experimental autoimmune encephalomyelitis in the common marmoset, a bridge between rodent EAE and multiple sclerosis for immunotherapy development. J Neuroimmune Pharmacol 2010;5:220–30
10. 't Hart BA, Laman JD, Bauer J, et al. Modelling of multiple sclerosis: Lessons learned in a non-human primate. Lancet Neurol 2004;3:588–97
11. Pomeroy IM, Matthews PM, Frank JA, et al. Demyelinated neocortical lesions in marmoset autoimmune encephalomyelitis mimic those in multiple sclerosis. Brain 2005;128:2713–21
12. Teeling JL, French RR, Cragg MS, et al. Characterization of new human CD20 monoclonal antibodies with potent cytolytic activity against non-Hodgkin lymphomas. Blood 2004;104:1793–800
13. Teeling JL, Mackus WJ, Wiegman LJ, et al. The biological activity of human CD20 monoclonal antibodies is linked to unique epitopes on CD20. J Immunol 2006;177:362–71
14. Kap YS, van Driel N, Blezer E, et al. Late B cell depletion with a human anti-human CD20 IgG1kappa monoclonal antibody halts the development of experimental autoimmune encephalomyelitis in marmosets. J Immunol 2010;185:3990–4003
15. Kap YS, Smith P, Jagessar SA, et al. Fast progression of recombinant human myelin/oligodendrocyte glycoprotein (MOG)–induced experimental autoimmune encephalomyelitis in marmosets is associated with the activation of MOG34–56-specific cytotoxic T cells. J Immunol 2008; 180:1326–37
16. Kerlero de Rosbo N, Hoffman M, Mendel I, et al. Predominance of the autoimmune response to myelin oligodendrocyte glycoprotein (MOG) in multiple sclerosis: Reactivity to the extracellular domain of MOG is directed against three main regions. Eur J Immunol 1997;27:3059–69
17. 't Hart BA, Hintzen RQ, Laman JD. Preclinical assessment of therapeutic antibodies against human CD40 and human interleukin-12/23p40 in a nonhuman primate model of multiple sclerosis. Neurodegener Dis 2008;5:38–52
18. Bleeker WK, Munk ME, Mackus WJ, et al. Estimation of dose requirements for sustained in vivo activity of a therapeutic human anti–CD20 antibody. Br J Haematol 2008;140:303–12
19. Blezer EL, Bauer J, Brok HP, et al. Quantitative MRI-pathology correlations of brain white matter lesions developing in a non–human primate model of multiple sclerosis. NMR Biomed 2007;20:90–103
20. 't Hart BA, Bauer J, Muller HJ, et al. Histopathological characterization of magnetic resonance imaging–detectable brain white matter lesions in a primate model of multiple sclerosis: A correlative study in the experimental autoimmune encephalomyelitis model in common marmosets (*Callithrix jacchus*). Am J Pathol 1998;153:649–63
21. Laman JD, van Meurs M, Schellekens MM, et al. Expression of accessory molecules and cytokines in acute EAE in marmoset monkeys (*Callithrix jacchus*). J Neuroimmunol 1998;86:30–45
22. Kooi EJ, Geurts JJ, van Horssen J, et al. Meningeal inflammation is not associated with cortical demyelination in chronic multiple sclerosis. J Neuropathol Exp Neurol 2009;68:1021–28
23. Trapp BD, Peterson J, Ransohoff RM, et al. Axonal transection in the lesions of multiple sclerosis. N Engl J Med 1998;338:278–85
24. von Büdingen HC, Tanuma N, Villoslada P, et al. Immune responses against the myelin/oligodendrocyte glycoprotein in experimental autoimmune demyelination. J Clin Immunol 2001;21:155–70
25. Matsushita T, Yanaba K, Bouaziz JD, et al. Regulatory B cells inhibit EAE initiation in mice while other B cells promote disease progression. J Clin Invest 2008;118:3420–30
26. Kutzelnigg A, Lassmann H. Cortical lesions and brain atrophy in MS. J Neurol Sci 2005;233:55–59
27. Bo L, Vedeler CA, Nyland H, et al. Intracortical multiple sclerosis lesions are not associated with increased lymphocyte infiltration. Mult Scler 2003;9:323–31
28. Brink BP, Veerhuis R, Breij EC, et al. The pathology of multiple sclerosis is location-dependent: No significant complement activation is detected in purely cortical lesions. J Neuropathol Exp Neurol 2005;64:147–55
29. van Horssen J, Brink BP, de Vries HE, et al. The blood-brain barrier in cortical multiple sclerosis lesions. J Neuropathol Exp Neurol 2007;66: 321–28

30. Bo L, Vedeler CA, Nyland HI, et al. Subpial demyelination in the cerebral cortex of multiple sclerosis patients. J Neuropathol Exp Neurol 2003;62:723–32
31. Magliozzi R, Howell O, Vora A, et al. Meningeal B-cell follicles in secondary progressive multiple sclerosis associate with early onset of disease and severe cortical pathology. Brain 2007;130:1089–104
32. Lucchinetti C, Bruck W, Parisi J, et al. Heterogeneity of multiple sclerosis lesions: Implications for the pathogenesis of demyelination. Ann Neurol 2000;47:707–17
33. Genain CP, Nguyen MH, Letvin NL, et al. Antibody facilitation of multiple sclerosis-like lesions in a nonhuman primate. J Clin Invest 1995; 96:2966–74
34. McFarland HI, Lobito AA, Johnson MM, et al. Determinant spreading associated with demyelination in a nonhuman primate model of multiple sclerosis. J Immunol 1999;162:2384–90
35. Jagessar SA, Kap YS, Heijmans N, et al. Induction of progressive demyelinating autoimmune encephalomyelitis in common marmoset monkeys using MOG34–56 peptide in incomplete Freund adjuvant. J Neuropathol Exp Neurol 2010;69:372–85
36. Weber MS, Prod'homme T, Patarroyo JC, et al. B-cell activation influences T-cell polarization and outcome of anti-CD20 B-cell depletion in central nervous system autoimmunity. Ann Neurol 2010;68: 369–83
37. Monson NL, Cravens P, Hussain R, et al. Rituximab therapy reduces organ-specific T cell responses and ameliorates experimental autoimmune encephalomyelitis. PLoS One 2011;6:e17103
38. Tedder TF, Klejman G, Disteche CM, et al. Cloning of a complementary DNA encoding a new mouse B lymphocyte differentiation antigen, homologous to the human B1 (CD20) antigen, and localization of the gene to chromosome 19. J Immunol 1988;141:4388–94
39. Duddy M, Niino M, Adatia F, et al. Distinct effector cytokine profiles of memory and naive human B cell subsets and implication in multiple sclerosis. J Immunol 2007;178:6092–99
40. Lund FE, Randall TD. Effector and regulatory B cells: Modulators of CD4(+) T cell immunity. Nat Rev Immunol 2010;10:236–47
41. Matsushita T, Horikawa M, Iwata Y, et al. Regulatory B cells (B10 cells) and regulatory T cells have independent roles in controlling experimental autoimmune encephalomyelitis initiation and late-phase immunopathogenesis. J Immunol 2010;185:2240–52
42. Bouaziz JD, Yanaba K, Venturi GM, et al. Therapeutic B cell depletion impairs adaptive and autoreactive CD4+ T cell activation in mice. Proc Natl Acad Sci USA 2007;104:20878–83
43. Hamel K, Doodes P, Cao Y, et al. Suppression of proteoglycan-induced arthritis by anti–CD20 B cell depletion therapy is mediated by reduction in autoantibodies and CD4+ T cell reactivity. J Immunol 2008;180: 4994–5003

